ChemPubSoc Europe

DOI: 10.1002/cbic.201700521

CHEMBIOCHEM Full Papers

VIP *Very Important Paper*

Kinetic Analysis of PRMT1 Reveals Multifactorial Processivity and a Sequential Ordered Mechanism

Jennifer I. Brown,[a] Timo Koopmans,[b] Jolinde van Strien,[c] Nathaniel I. Martin,*[b] and Adam Frankel*[a]

Arginine methylation is a prevalent post-translational modification in eukaryotic cells. Two significant debates exist within the field: do these enzymes dimethylate their substrates in a processive or distributive manner, and do these enzymes operate using a random or sequential method of bisubstrate binding? We revealed that human protein arginine *N*-methyltransferase 1 (PRMT1) enzyme kinetics are dependent on substrate sequence. Further, peptides containing an *N*η-hydroxyarginine generally demonstrated substrate inhibition and had improved K_M values, which evoked a possible role in inhibitor design. We also revealed that the perceived degree of enzyme processivity is a function of both cofactor and enzyme concentration, suggesting that previous conclusions about PRMT sequential methyl transfer mechanisms require reassessment. Finally, we demonstrated a sequential ordered Bi–Bi kinetic mechanism for PRMT1, based on steady-state kinetic analysis. Together, our data indicate a PRMT1 mechanism of action and processivity that might also extend to other functionally and structurally conserved PRMTs.

Introduction

Arginine-methylated proteins are involved in many important cellular functions, including RNA processing, epigenetic transcription regulation, signal transduction, and DNA repair.[1] Considering that approximately 0.5% of arginine residues in the human proteome are methylated, this post-translational modification is thought to be a major regulatory element.[2,3] Therefore, arginine methylation profiles of proteins need to be under strict control by maintenance enzymes to ensure proper cellular function. One method of regulating arginine methylation is through demethylases. Jumonji domain-containing 6 (JMJD6) protein oxygenase was previously identified as an arginine demethylase in humans; however, its demethylation activity has not been substantiated.[4,5] In contrast, the enzymes responsible for arginine methylation have been well characterized.

Protein arginine *N*-methyltransferase (PRMT) enzymes are responsible for post-translationally methylating the guanidine moiety of specific arginine residues in target protein substrates while, in the process, converting the methyl donor *S*-adenosyl-L-methionine (SAM) into *S*-adenosyl-L-homocysteine (SAH). Nine members of the human PRMT family are categorized based on the type of methylated product(s) each forms: type I enzymes (PRMT1–4, PRMT6, and PRMT8) catalyze the formation of *N*η-monomethyl- and asymmetric *N*η,*N*η-dimethylarginine (MMA and aDMA, respectively); type II enzymes (PRMT5 and PRMT9) catalyze the formation of MMA and symmetric *N*η1,*N*η2-dimethylarginine (sDMA); and the type III enzyme PRMT7 is only able to form MMA (Scheme 1).[6–14] Many groups have demonstrated that active site steric interactions surrounding the substrate arginine residue contribute to enzyme product specificity. For example, changes to one or two residues within the PRMT1 active site have been shown to either alter the distribution of MMA and aDMA products or shift the enzymatic regioselectivity from aDMA to sDMA.[15–17] This regioselective shift from one or two amino acid changes was also observed in PRMT7 from *Trypanosoma brucei*, in which an E181D variant expanded this enzyme's product formation to include aDMA, and a E181D/ Q329A double variant formed sDMA.[18,19] Two native glutamate residues in PRMT7 (E181 and E172) demarcate an invariant "double E loop" that coordinates the positive charge of arginine within the active site. Glutamic acid to glutamine conversions within the double E loop have been shown to compromise enzyme activity in different PRMTs,[19–22] underscoring the functional importance of this conserved sequence motif.

Another conserved and notable sequence motif within the PRMT active site is referred to as the THW loop. Variations on this sequence motif specific for each PRMT product type were demonstrated in the mutagenesis study of *Tb*PRMT7, as well as identified in a recent structural study of PRMT6.[19,23] As prod-

[a] *J. I. Brown, Dr. A. Frankel*
Faculty of Pharmaceutical Sciences, University of British Columbia
2405 Wesbrook Mall, Vancouver, BC V6T 1Z3 (Canada)
E-mail: adam.frankel@ubc.ca

[b] *Dr. T. Koopmans, Dr. N. I. Martin*
Department of Chemical Biology and Drug Discovery
Utrecht Institute for Pharmaceutical Sciences, University of Utrecht
3584 CG Utrecht (The Netherlands)
E-mail: n.i.martin@uu.nl

[c] *J. van Strien*
Leiden Institute for Chemistry, Gorlaeus Laboratories
Einsteinweg 55, 2333CC Leiden (The Netherlands)

Supporting information and the ORCID identification numbers for the authors of this article can be found under https://doi.org/10.1002/cbic.201700521.

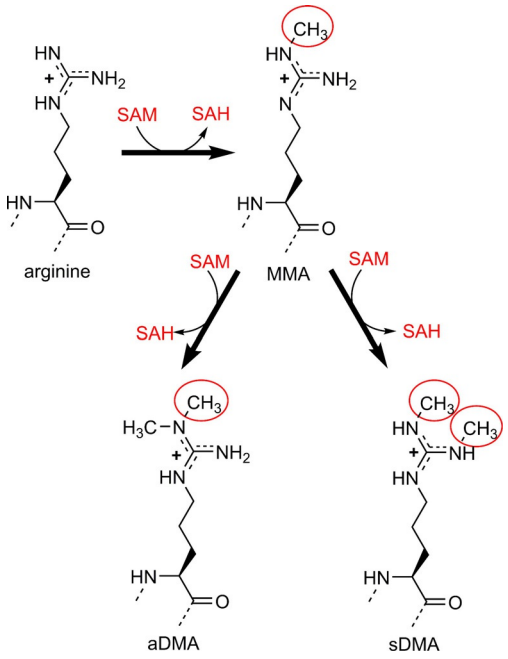

Scheme 1. Production of methylarginine species. PRMTs use *S*-adenosyl-L-methionine (SAM) as a cofactor to donate methyl groups (red circle) to produce monomethylated arginine (MMA) and the spent cofactor *S*-adenosyl-L-homocysteine (SAH). Substrates might undergo subsequent rounds of methylation to form asymmetric or symmetric dimethylarginine (aDMA or sDMA).

uct specificities of PRMTs appear tunable through mutagenesis and diverge merely due to a small number of active site residue differences, it is likely that all PRMTs share a common catalytic mechanism, regardless of enzyme type.

The presence of conserved structural motifs in PRMTs provides further evidence to support a common mechanism. PRMTs contain a seven-β-strand structural motif that is representative of the largest superfamily of SAM-dependent methyltransferases.[24] This Rossmann-like structural core makes several conserved contacts with SAM and, in PRMTs, several pieces of structural evidence suggest that cofactor binding induces a conformational change within the enzyme, whereby an N-terminal α-helix buries it within the interior of the protein and, as a consequence, completes the formation of the nearby peptide-binding groove.[23,25–29] Binding studies between PRMTs and either peptides or small-molecule inhibitors (ligands that bind in the peptide-binding groove) using isothermal titration calorimetry (ITC) have demonstrated cofactor (SAM or SAH) dependence in order to elicit a binding isotherm, which supports a sequential order of substrate binding to enzyme.[27,30–34] Despite mechanistic implications surrounding these observations, enzyme kinetic studies of different PRMTs have generated conflicting data as to whether SAM binding precedes peptide substrate binding (i.e., sequential ordered mechanism) or not (i.e., random mechanism). Interpretations of kinetic and molecular modeling data for PRMT1,[11,32,35–37] CARM1,[27,38] PRMT5,[39,40] and PRMT6[23,31,41,42] have varied between sequential and random mechanisms. Therefore, further kinetic and structural research into these enzymes needs to be performed while considering the extent of the published literature to help settle this debate and establish consensus on a shared PRMT mechanism.

The dimerization arm that extends from the C-terminal β-barrel domain is another shared structural motif within the PRMT enzyme family whose function suggests a common mechanism. For most PRMTs, crystal structures show that the dimerization arm of one subunit makes reciprocal contacts with the other subunit to form an overall toroidal shape in which the two active sites face inward and across from one another.[20,25,26,28,31,40,43–47] In the absence of a dimerization arm, recombinantly expressed versions of mammalian PRMT1 and its yeast homologue Rmt1p/Hmt1p are monomeric, unable to bind to SAM, and inactive.[20,48] CARM1 phosphorylation at a conserved serine residue near the dimer interface was shown to inhibit dimerization and prevent SAM binding, thereby regulating enzyme function during cell cycle progression.[49] In addition to dimerization being a requirement for SAM binding, our group found that SAM and SAH influenced the dissociation constants for PRMT1 and PRMT6 homodimers.[50] PRMT dimerization and its relationship with cofactor binding, therefore, are undoubtedly important aspects of enzyme activity.

One of the aspects of enzyme activity for which consensus has not been established in the literature is in the sequential transfer of methyl groups onto a single substrate arginine residue (i.e., dimethylation). A processive enzyme, in this instance, does not release the substrate prior to the second methylation in aDMA or sDMA formation, whereas a distributive enzyme releases substrate after the first methylation to give MMA as the predominant product. Several studies offer compelling data and rationales in support of processive or distributive mechanisms for PRMT1,[11,32,36,37,41,51–54] PRMT2,[11] PRMT3,[54] CARM1,[38] PRMT5,[39,55–57] PRMT6,[6,41,42] PRMT7,[44] and PRMT9.[19]

The purpose of the current research was to use steady-state enzyme kinetics to further explore PRMT1's methylation activity, in terms of catalytic mechanism and degree of processivity, with several biologically relevant peptide substrates. Our lab previously studied the effect of univalent isosteric replacement of the methyl group in MMA with a hydroxy substituent, which lowered the pK_a of the arginine guanidino group from 12.5 to 8.7, and found that it was amenable to methylation.[58] Here, we demonstrate that hydroxy-substituted substrates behave similarly to monomethylated substrates and, in the context of the H4 peptide, result in the strongest substrate inhibition. We also demonstrate, in congruence with previous findings, that the degree of enzyme processivity is substrate dependent. Additionally, we show, for the first time, that the degree of processivity was dependent on cofactor and enzyme concentrations. Finally, we demonstrate that PRMT1 acts in a sequential ordered Bi–Bi mechanism, which differs from recently reported findings.[36,38] These results are significant in that they provide for a better understanding of how PRMT1 catalyzes sequential methylation reactions. These insights likely extend to other PRMT family members.

Results and Discussion

PRMT1 kinetics are dependent on substrate sequence

We first sought to investigate single and double methyl transfers by PRMT1 on well-characterized peptide substrates due to a lack of consensus regarding the enzyme kinetic mechanism of PRMT1. Unmethylated, monomethylated, and hydroxylated versions of peptides representing the following PRMT1 substrates were studied: histone H4 (H4), eukaryotic initiation factor (eIF4A1), and two fibrillarin-based peptides (KRK and RKK).[59–63] An acetylated version of the fibrillarin-based (R1) peptide from our previous study on arginine isosteres[58] was used as a reference substrate for comparison with other peptide sequences (Table 1). The hydroxylated peptides were used to investigate the differences in PRMT1 kinetics between monomethylated and hydroxylated isosteric substrates.

Table 1. Peptide substrates synthesized to contain either an unmodified arginine residue or an *N*η-hydroxyl-, *N*η-monomethyl-, or *N*η,*N*η-dimethyl-substituted arginine residue (shown in bold).

Peptide	Sequence
H4	Ac-SG**R**GKGGKGLGKGGAKR
H4-CH_3	Ac-SG$\mathbf{R_{Me}}$GKGGKGLGKGGAKR
H4-OH	Ac-SG$\mathbf{R_{OH}}$GKGGKGLGKGGAKR
eIF4A1	Ac-YIHRIG**R**GGR
eIF4A1-CH_3	Ac-YIHRIG$\mathbf{R_{Me}}$GGR
eIF4A1-OH	Ac-YIHRIG$\mathbf{R_{OH}}$GGR
KRK	Ac-KGGFGG**R**GGFGGKW
KRK-CH_3	Ac-KGGFGG$\mathbf{R_{Me}}$GGFGGKW
KRK-OH	Ac-KGGFGG$\mathbf{R_{OH}}$GGFGGKW
RKK	Ac-GG**R**GGFGGKGGFGGKW
RKK-CH_3	Ac-GG$\mathbf{R_{Me}}$GGFGGKGGFGGKW
RKK-OH	Ac-GG$\mathbf{R_{OH}}$GGFGGKGGFGGKW
RKK-$(CH_3)_2$	Ac-GG$\mathbf{R_{Me2a}}$GGFGGKGGFGGKW
R1	Ac-WGGYS**R**GGYGGW

The rate of methyl transfer was assessed by quantifying the incorporation of radiolabeled methyl groups into peptides in a p81 filter binding assay, except in the case of the R1 peptide, where we measured radioactivity in gel slices. In all cases, 200 nM of purified PRMT1 (Figure S1 in the Supporting Information) and 50 μM SAM were used, which is a saturating condition (the K_M value for SAM is 1.0 μM).[11] Reactions were performed for one hour, within the linear range of the enzyme (Figure S2 in the Supporting Information). The rate values were fitted to Michaelis–Menten Equation (1) or (2), from which the apparent V_{max} (pmol min^{-1}, normalized to nmol enzyme), K_M, and k_{cat} values were estimated. We found that for almost all of the peptide substrates, PRMT1 displays the highest activity towards the unmodified peptides. Specifically, unmodified eIF4A1, KRK, and RKK peptides exhibit the highest V_{max} values, whereas the monomethylated and hydroxylated isosteres reveal comparably lower V_{max} values (Figure 1 and Figure S3 in the Supporting Information).

These observations were expected, because monomethylated and hydroxylated substrates are sterically similar and allow for only one methyl transfer at the methylation site. However, unmodified and monomethylated H4 peptides exhibited similarly high apparent V_{max} values, whereas the value for the hydroxylated peptide was unexpectedly and appreciably lower. This result indicates that PRMT1 had similar catalytic activity towards unmodified and modified H4 substrates alike, which is revealed by their comparable K_M and k_{cat} values (Table 2). Furthermore, although PRMT1 appears to display approximately twofold higher catalytic efficiency (k_{cat}/K_M) towards hydroxylated H4 and eIF4A1 peptide substrates compared to their monomethylated counterparts, PRMT1 catalysis is less efficient for the hydroxylated KRK and RKK substrates (Table 2). A consistently observed trend, however, is that PRMT1 requires less hydroxylated substrate to achieve half-maximal velocity compared to its unmodified and monomethylated counterparts, as observed by the lower apparent K_M values for each hydroxylated peptide. The failure to observe a predicted increase in turnover number for all hydroxylated peptides suggested that the presence of the *N*η-hydroxyarginine had differential effects on PRMT1 catalysis, based on peptide sequence context, underscoring substrate-dependent effects on PRMT1 enzyme kinetics seen previously with unmodified and monomethylated forms of these peptides.[53]

It was further observed that some datasets fit better to a modified Michaelis–Menten inhibition model [Eq. (2)]. As seen in Figure 1 and Table 2, H4-OH, eIF4A1-OH, KRK, KRK-CH_3, KRK-OH, RKK-CH_3, and RKK-OH display an inhibitory effect on PRMT1 catalysis at higher substrate concentrations. The hydroxylated KRK and eIF4A1 peptides exhibit some substrate inhibition, but did not adequately fit to the inhibition model from which K_i values were derived. Generally, K_i values for peptides are high, but variable depending on the peptide sequence. It is unclear why some peptides lead to an inhibitory effect, but we have previously observed that the substrate inhibition effect can be mitigated by increasing enzyme concentration.[64] Therefore, we performed steady state kinetics experiments on the H4-OH peptide at different PRMT1 concentrations and found that doubling or quadrupling the enzyme concentration to 400 or 800 nM eradicates substrate inhibition (Figure S4). Additionally, different PRMT1 concentrations display different kinetic parameters (Table S2) similar to what has been shown for methylation activity towards unmodified histone H4 and Tat peptides.[35,64]

PRMT1 kinetic data with the unsubstituted H4 peptide presented here are consistent with data presented by Dillon et al., with all calculated apparent enzyme kinetic values falling within the same order of magnitude.[65] This previous publication used a radioactive gel-based assay, comparable to what we used to calculate apparent kinetic data for the R1 peptide. The apparent K_M, k_{cat}, and k_{cat}/K_M values for unmodified and monomethylated eIF4A1, KRK, and RKK peptides differed compared to what has been reported by Hevel and co-workers by an order of magnitude.[53] Whereas Gui et al. reported an apparent higher catalytic efficiency for each monomethylated peptide compared to its unmethylated counterpart,[53] we only observed a higher catalytic efficiency for the monomethylated RKK peptide. Many experimental design variations could con-

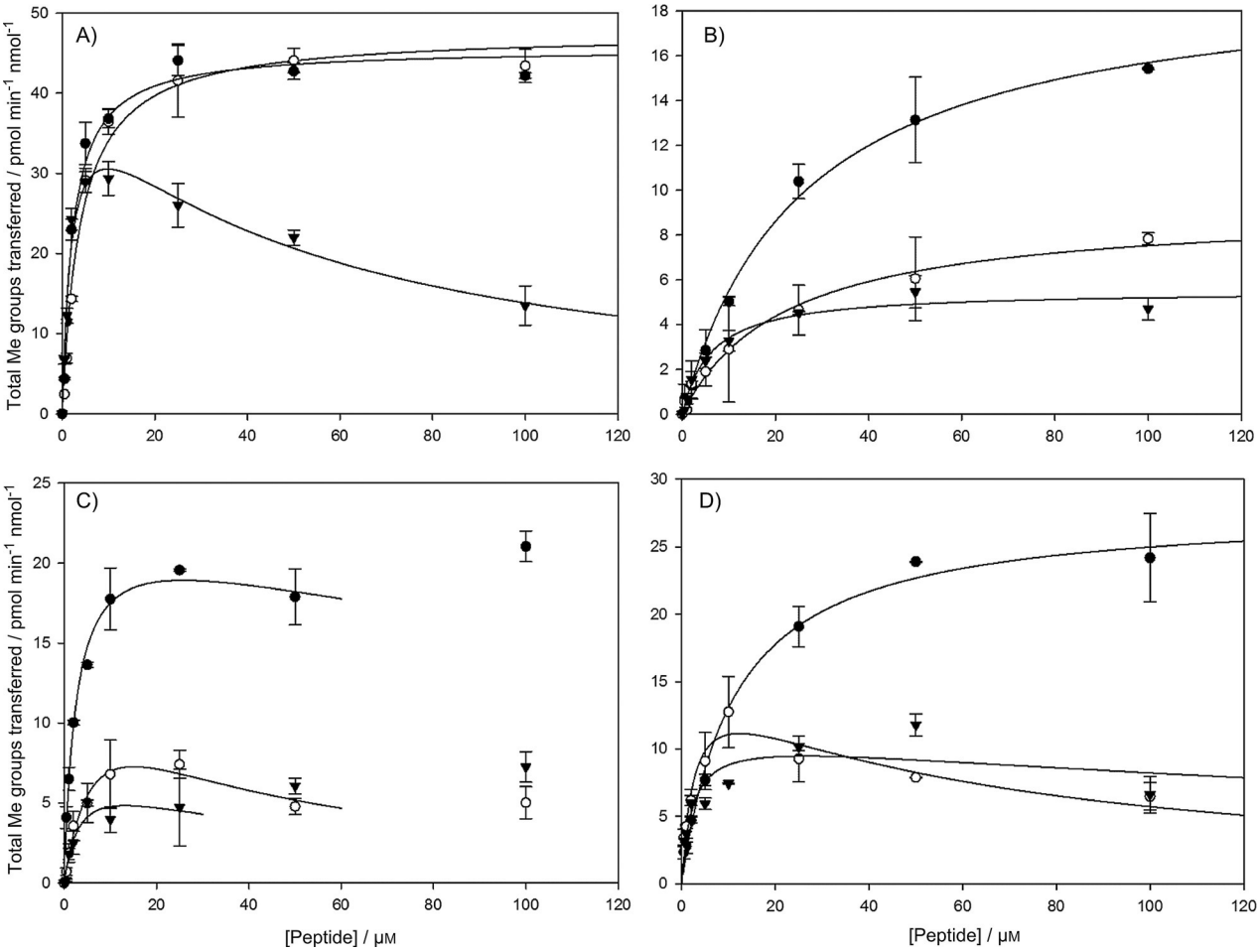

Figure 1. Michaelis–Menten enzyme kinetics of PRMT1 methylation of peptide substrates. Reactions containing 200 nM PRMT1, 50 μM SAM, and varying concentrations of unmodified (●), monomethylated (○), or hydroxylated (▼) A) H4, B) eIF4A1, C) KRK, or D) RKK peptides were monitored for methyl transfer activity over 1 h at 37 °C. Data points were fit to the Michaelis–Menten equation. Error bars represent standard error ($n = 2$).

tribute to these differences. Our methodology included a radioactive assay approach, compared to a continuous spectrophotometric assay. In our assay, all background automethylation of the enzyme was subtracted based on an enzyme-only reaction, whereas the continuous spectrophotometric assay accounted for both substrate methylation and enzyme automethylation. The limit of detection of our radiometric assay was approximately 0.1 pmol of methyl groups transferred, compared to a 10 pmol limit of detection (10 μM in a 1.0 cm cuvette) reported for the continuous spectrophotometric assay.[53] The lower limit of detection for our assay allowed us to collect data over a broad range of substrate concentrations, leading to a comprehensive curve when fit to the Michaelis–Menten equation. Furthermore, the enzyme concentrations used (200 nM in this study versus 4.0 μM) might also contribute to these differences. Finally, Gui et al. used SAH nucleosidase and adenine deaminase to decompose SAH and prevent its feedback inhibition of PRMT1 in their assay, which might have also contributed to differences between our apparent kinetic parameters.

Our substrate inhibition data support, in part, an inhibition theory proposed by Zheng and co-workers, who suggested that substrate inhibition could be due to the accumulation of a binary or ternary complex with the enzyme that has not undergone a conformational change and is, therefore, catalytically inactive.[32] Their analysis did not take into account that substrate inhibition was observed at low enzyme concentrations. We have previously argued that PRMT1 in solution contains concentration-dependent enzyme populations in various oligomeric states whose kinetic behaviors differ.[64] At a lower enzyme concentration, PRMT1 was susceptible to substrate inhibition, whereas at a high concentration—well above the K_D value of dimerization (110 nM)[50]—a kinetically distinct PRMT1 population was no longer susceptible to substrate inhibition. As the inhibition effect on H4-OH peptide is alleviated at higher enzyme concentrations, our results further support our prevailing theory.

In summary, PRMT1 displays the highest catalytic activity towards unmodified peptide substrates, whereas it methylates hydroxy-substituted peptides comparably to their monomethylated isosteres (with the exception of the H4 peptide). For some peptide substrates, including some hydroxylated peptides, PRMT1 kinetics modelled to substrate inhibition. Taken together, these data suggest that the enzyme kinetics of

Table 2. Apparent enzyme kinetic parameters of PRMT1 with unmethylated, monomethylated, and hydroxylated H4, eIF4A, KRK, and RKK peptides, as well as unmodified R1 peptide.

Peptide	K_M [μM]	k_{cat} ($\times 10^{-4}$) [s^{-1}]	k_{cat}/K_M ($\times 10^{-2}$) [M^{-1} s^{-1}]	K_i [μM]
H4	2.30 ± 0.36	7.60 ± 0.27	330 ± 53	–
H4-CH_3	3.94 ± 0.58	7.92 ± 0.28	202 ± 30	–
H4-OH	2.03 ± 0.49	7.20 ± 0.73	355 ± 93	47.6 ± 12
eIF4A1	25.9 ± 2.6	3.30 ± 1.3	12.7 ± 5.3	–
eIF4A1-CH_3	22.0 ± 3.9	1.53 ± 0.10	6.97 ± 1.3	–
eIF4A1-OH	6.17 ± 1.1	0.92 ± 0.05	14.9 ± 2.8	[a]
KRK	2.64 ± 0.40	3.80 ± 0.23	144 ± 67	250 ± 120
KRK-CH_3	4.48 ± 1.8	1.75 ± 0.33	39 ± 17	72.5 ± 34
KRK-OH	3.35 ± 1.1	0.97 ± 0.08	28.8 ± 10	[a]
RKK	11.3 ± 1.3	4.63 ± 1.5	41.0 ± 14	–
RKK-CH_3	2.70 ± 1.1	2.67 ± 0.48	98.8 ± 43	56.5 ± 25
RKK-OH	2.25 ± 1.6	1.85 ± 0.45	82.2 ± 60	309 ± 470
R1	141 ± 30	4.57 ± 0.65	3.23 ± 0.82	–
H4	2.30 ± 0.36	7.60 ± 0.27	330 ± 53	–

Values ± standard error of two replicates are shown. [a] Data did not fit to inhibition model.

PRMT1 vary and are affected by substrate sequence, which complements what was seen by Hevel and co-workers,[53] and arginine modification. The finding that arginine hydroxylation generally led to an inhibitory effect, as well as to a largely improved K_M value compared to unmodified counterparts, could suggest a benefit to using hydroxy groups in potential PRMT1 active site inhibitor design.

PRMT1 degree of processivity increases with both cofactor and enzyme concentration

Our observation that PRMT1 displays differential apparent kinetic parameters based on substrate identity led us to speculate that peptide substrates might also affect the level of methylated product. Therefore, we aimed to discern relative amounts of MMA and aDMA produced on each unmodified substrate under various experimental conditions. We first investigated the ratio of MMA and aDMA produced on saturating concentrations of unmodified peptide substrates under conditions used for steady-state kinetics experiments described above (methylation reactions for 1 h with 200 nM PRMT1, 50 μM SAM, 100 μM peptide). We expected to see different aDMA/MMA ratios if PRMT1 activity was dependent on substrate sequence, which has previously been shown for these peptides.[53] We found that for eIF4A1, KRK, and RKK peptide substrates, approximately 1.4-fold more MMA was produced than aDMA after 1 h, whereas 4.4-fold more MMA was produced than aDMA on the H4 peptide substrate (data not shown). These different observed ratios brought into question the effect of substrate sequence on enzyme processivity. Given the experimental conditions and reaction time within the linear range, a processive PRMT1 would predominantly produce dimethylarginine, whereas a distributive PRMT1 would mostly produce monomethylarginine, with the dimethylarginine species accumulating only after the concentration of monomethylated substrate rose to the level of the unmodified substrate concentration. An enzyme that produces an appreciable amount of both the monomethylated and dimethylated species might be described as acting semi-processively.[36] Using these definitions, we find PRMT1 acting distributively towards the H4 peptide and semi-processively towards the eIF4A1, KRK, and RKK peptides under the described experimental conditions.

We designed additional experiments to measure the amount of enzyme processivity under limiting or excess concentrations of SAM and unmodified peptides. Methylation reactions were performed in which SAM was limiting (1.0 μM) and peptides were in excess (10 K_M), SAM was twofold (10 μM) in excess of enzyme concentration and peptides were in excess (10K_M), and finally, SAM was in excess (100 μM) and peptides were limiting (10 μM). The degree of processivity was assessed by measuring aDMA/MMA ratios. Enzyme was removed from each methylation reaction and the remaining methylated targets were acid hydrolyzed to individual amino acid components. Ratios were quantified by using ultra-high-performance liquid chromatography tandem mass spectrometry (UHPLC-MS/MS). The limit of detection for aDMA and MMA from the 60 μL reaction volume with this method is 1.2 pmol and 0.6 pmol, respectively. In order to ensure that we observed enough product to accurately quantify, we used 5.0 μM PRMT1 in these reactions.

For each peptide, MMA and aDMA were produced with various aDMA/MMA ratios by PRMT1 under different conditions tested (Figure 2 and Table 3). The H4 peptide yielded aDMA/MMA ratios of 5.0:1 and 7.2:1 for SAM-intermediate and SAM-excess conditions, respectively, which is an appreciably higher ratio than what we see for the other three substrates. These conditions suggest that PRMT1 acts more processively towards the H4 substrate peptide than it does towards other tested substrates. Under SAM-limiting conditions, the level of PRMT1 processivity was strikingly different from SAM-intermediate and SAM-excess conditions. In this case, both the H4 and KRK peptide substrates yielded approximately twofold more monomethylated than dimethylated product, whereas eIF4A1 and RKK peptide substrates bear approximately equal levels of both methylarginine species. PRMT1 appears to behave less processively towards H4 and KRK under SAM limiting conditions. Together, these results demonstrate that relative SAM concentration directly affects PRMT1 processivity, whereas the peptide concentration does not.

We turned our attention to the effect of enzyme concentration on processivity by testing different PRMT1 concentrations with constant saturating levels of SAM and peptide. Our results show that the aDMA/MMA ratio increases for each peptide with a concomitant increase in PRMT1 concentration (Figure 3 and Table 4), demonstrating that PRMT1 processivity is directly linked to enzyme concentration. Additionally, these results show that the increase in aDMA disproportionally contributes to the overall increase in methylated product as compared to MMA at the highest enzyme concentration tested. This result supports the notion that PRMT1 processivity is a function of enzyme concentration.

Our observations that both cofactor and enzyme concentration affect PRMT1 processivity led us to question what influen-

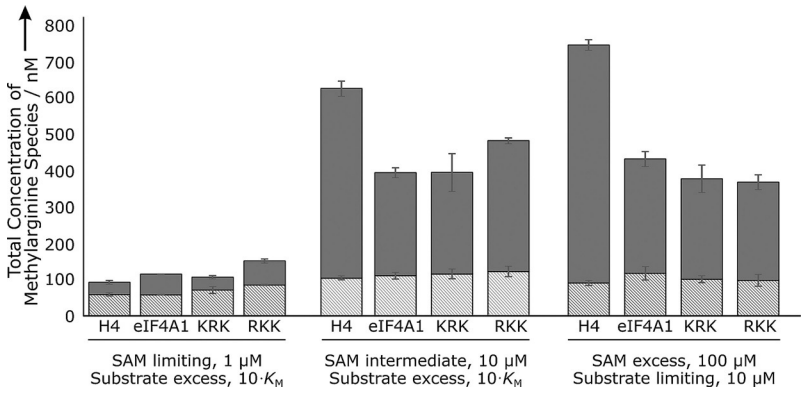

Figure 2. PRMT1 degree of processivity for substrate peptides. Reactions containing 5.0 μM PRMT1 and the indicated concentrations of SAM and unsubstituted peptides were incubated at 37 °C for 1 h. PRMT1 was removed from the sample to eliminate automethylation, and remaining methylated targets were acid hydrolyzed. Concentrations of aDMA (dark gray) and MMA (light gray) were determined by UHPLC-MS/MS. Error bars represent standard deviation ($n = 3$).

Table 3. PRMT1 degree of processivity for substrate peptides.

	Limiting SAM, excess peptide			Intermediate SAM, excess peptide			Excess SAM, limiting peptide		
Peptide	aDMA	MMA	Ratio	aDMA	MMA	Ratio	aDMA	MMA	Ratio
H4	33.6 ± 5.5	58.8 ± 3.7	1:1.8	543 ± 22	108 ± 5.5	5.0:1	657 ± 15	91.0 ± 7.0	7.2:1
eIF4A1	57.3	57.8	1:1.0	294 ± 15	115 ± 9.6	2.6:1	316 ± 21	118 ± 19	2.7:1
KRK	35.5 ± 4.5	71.1 ± 9.4	1:2.0	290 ± 54	120 ± 14	2.4:1	277 ± 38	101 ± 9.5	2.7:1
RKK	66.5 ± 5.2	85.2 ± 1.3	1:1.3	374 ± 7.6	127 ± 15	2.9:1	271 ± 21	98.1 ± 16	2.8:1

aDMA/MMA ratios were determined for reactions as described in Figure 2. Values are listed as nM concentrations (± standard deviation of three replicates), and ratios are listed as aDMA/MMA.

ces the degree to which PRMT1 acts processively. From a mechanistic point of view, we know that higher concentrations of PRMT1 revealed a correspondingly increased level of dimerization and higher order oligomers.[35,50] Therefore, we hypothesized that factors that enhance enzyme dimerization might in turn increase processivity. We previously showed through FRET measurements that the addition of excess SAM lowered the K_D value of dimerization between mCer-PRMT1 and mCit-PRMT1.[50] Here, we used this FRET pair to determine how dimerization was affected by different concentrations of cofactor and peptide alone or in combination in an effort to better understand PRMT1 behavior and establish a model for its activity (Figure 4). To our surprise, we found that PRMT1 dimerization increased in response to increased concentrations of SAM, SAH, or KRK peptide. At the highest concentrations, KRK appeared to cause the greatest increase in FRET signal as compared to SAM or SAH cofactor. Interestingly, the addition of both KRK peptide and SAM reveal an additive effect on FRET signal, thus suggesting that the PRMT1:SAM:peptide complex best promotes an equilibrium shift in favor of PRMT1 dimeriza-

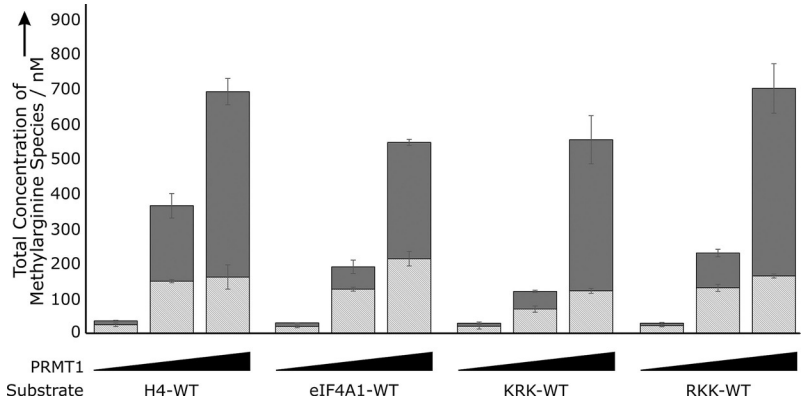

Figure 3. PRMT1 degree of processivity, varying enzyme concentration. Reactions containing 0.2, 1.0, or 5.0 μM PRMT1, 100 μM SAM, and peptide substrate (at least tenfold higher concentration than the K_M value: 25 μM for H4, 300 μM for eIF4A1, 35 μM for KRK, and 130 μM for RKK) were incubated for 1 h at 37 °C. Methylated peptide targets were acid-hydrolyzed and analyzed by UHPLC-MS/MS to quantify aDMA (dark gray) or MMA (light gray). Error bars represent standard deviation ($n = 3$).

Table 4. PRMT1 degree of processivity with various enzyme concentrations.

	0.2 μM PRMT1			1.0 μM PRMT1			5.0 μM PRMT1		
Peptide	aDMA	MMA	Ratio	aDMA	MMA	Ratio	aDMA	MMA	Ratio
H4	11.1 ± 1.5	25.4 ± 5.2	1:2.3	215 ± 35	150 ± 4.5	1.4:1	529 ± 38	162 ± 34	3.3:1
eIF4A1	10.2 ± 0.31	21.6 ± 4.0	1:2.12	63.4 ± 19	128 ± 5.7	1:2.0	332 ± 8.5	215 ± 21	1.6:1
KRK	8.65 ± 3.4	19.9 ± 8.0	1:2.3	50.4 ± 3.5	21.4 ± 8.9	1:1.4	431 ± 69	121 ± 7.0	3.6:1
RKK	7.05 ± 2.0	23.8 ± 3.3	1:3.4	98.9 ± 11	132 ± 10	1:1.3	535 ± 71	166 ± 5.9	3.2:1

aDMA/MMA ratios were determined for reactions described in Figure 3. Values are listed as nanomolar concentrations (± standard deviation of three replicates), and ratios are listed as aDMA/MMA.

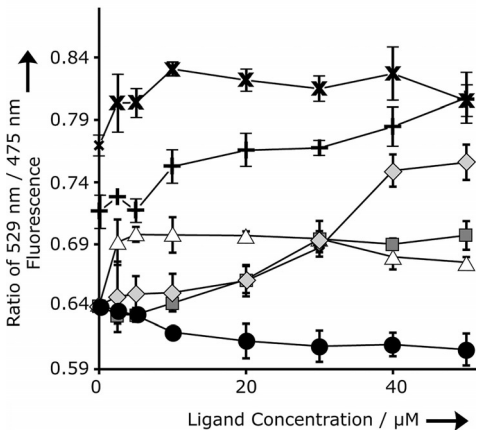

Figure 4. Cofactor and peptide contribution to PRMT1 dimerization. The FRET signal for PRMT1 dimerization, as measured by using both mCer- and mCit-PRMT1 (100 nM each), increases in the presence of KRK (◆), SAM (■), or SAH (△) alone, as well as in the presence of increasing KRK and constant SAM concentrations (+), or increasing SAM and constant KRK concentrations (**x**). Buffer control (●). Error bars represent standard deviation ($n = 3$).

tion, which might represent a mechanism by which PRMT1 processivity proceeds.

Although we were the first group to identify that SAM concentration affects the level of PRMT processivity, this study is not the first published example. Other studies of PRMT1 and PRMT5 have shown that higher SAM concentrations can lead to more aDMA and sDMA, respectively, even though SAM was not implicated as a possible cause.[53,55] Similarly, although we were the first to explicitly show that enzyme concentration affects processivity, our conclusion is actually well represented in published studies that have classified different PRMT enzymes as acting processively or distributively.[6,11,19,32,36–39,42,51–55] Not only does the lack of consensus in the literature suggest that PRMT kinetics could be dependent on substrate identity, but our current findings also demonstrate that inherent differences in experimental design, such as enzyme and cofactor concentration, contribute to observed differences regarding distributive or processive mechanisms. For example, our group, as well as Wahle and co-workers, have concluded that PRMT1 acts distributively when tested at low nanomolar concentrations.[11,54] Other groups found PRMT1 to act semi-processively at higher nanomolar and micromolar concentrations.[51,53] Therefore, conclusions drawn about PRMT processivity in the literature are largely consistent and predictable, based on cofactor and enzyme concentrations used in the assay.

Based on our product formation and FRET results, we theorized that PRMT1 dimerization might explain how the enzyme is capable of performing processively. Most processive enzymes are toroidal in shape and bear a central cavity containing one or more active sites.[66] PRMT dimers share this structural feature[20,48,67] and are capable of processive arginine dimethylation under certain assay conditions, as discussed above. It is, however, uncertain exactly how PRMT dimers behave processively. With two active sites per PRMT dimer, it is tempting to speculate that each site contributes to arginine dimethylation. This notion is supported by the fact that the stoichiometry of ligand binding to PRMT6 was shown by native mass spectrometry to be 2:2:1 for the PRMT6:SAH:peptide ternary complex.[28] However, we previously showed that mixed dimers of 25 nM active PRMT1 and 750 nM inactive (E153Q) PRMT1 formed approximately twofold more aDMA than MMA on full-length histone H4 after a 1 h reaction, providing some evidence that processive dimethylation can occur at one active site.[21] More recently, different amino acid residue changes within the one viable active site of PRMT7 converted it from a type III enzyme to a type I or type II enzyme,[18,19] thus providing additional evidence that dimethylation can occur at one active site. What remains unclear is how the target arginine can remain in one active site for two rounds of methylation, which might not necessarily be a prerequisite for processivity. PRMT1 has been shown to contain, in addition to the peptide binding groove adjacent to the active site, two additional exosite binding grooves that interact with substrate polypeptides.[20] It is plausible that these exosites could prevent substrates from completely dissociating from the enzyme after the first methylation event. This rationale is supported by the observation that histone H4 peptide length and distal elements were shown to strongly influence the catalytic efficiency of PRMT1,[51] indicating that binding interactions outside the active site are important for methylation.

Overall, the results from this set of experiments shine a new light on our understanding of PRMT1 processivity. We conclude that PRMT1 processivity is a multifactorial effect. Although the degree of PRMT1 processivity can depend on peptide substrate sequence identity,[53] we found that it is not affected by peptide concentration. Instead, we determined that enzyme and cofactor concentrations are the primary variables affecting apparent enzyme processivity. Although we only report this effect for PRMT1, it is logical to extend these considerations in determining processivity of other type I and type II arginine methyltransferases.

PRMT1 uses a sequential ordered Bi–Bi mechanism of action

A series of product inhibition experiments were designed to observe the effect of SAH and RKK-aDMA inhibitors on PRMT1 activity in the presence of varying SAM or RKK substrates by using the radiometric p81 filter binding assay. Transferred methyl groups were used to calculate the enzyme rate of reaction. Each dataset was fit to nonlinear models for competitive [Eq. (3)], uncompetitive [Eq. (4)], noncompetitive [Eq. (5)], and mixed [Eq. (6)] inhibition. Data sets were assessed as best fitting to models based on the best coefficient of determination and the lowest error. Data were also qualitatively presented in Eadie–Hofstee plots (rate versus rate/substrate), double-reciprocal Lineweaver–Burk plots (reciprocal rate versus reciprocal substrate), and Hanes–Woolf plots (substrate/rate versus substrate) for each product inhibitor concentration. These plots aided in determining which model best fit the data in some instances in which nonlinear regression analyses provided similar accuracy of fit and errors for multiple inhibition equations. The combination of these three plots gave a clear indication of the observed trend, rather than relying solely on the commonly used Lineweaver–Burk plot, which overemphasizes the data values collected at various low substrate concentrations, thereby heavily weighting regression of the line and enlarging the error.[68] Two leading kinetic mechanisms—rapid equilibrium random mechanism with dead-end EAP/EBQ complexes (ternary complexes comprising enzyme bound to one substrate and one product) and sequential ordered mechanism—were considered (Table 5). These kinetic mechanisms both have well-established and characteristic product inhibition patterns.[69] Our product inhibition data were analyzed to determine which mechanism was best supported by our results.

First, with increasing concentrations of SAH and varying SAM concentrations at 25 and 130 μM concentrations of RKK peptide, data sets best fit to a competitive model, suggesting that SAH displays competitive inhibition towards PRMT1 under these conditions (Table S3). Consistent with this analysis, all three linear plots also reveal a competitive inhibition pattern (Figure 5 A and B), in which apparent V_{max} does not change, but apparent K_M increases with increasing inhibitor concentration. As SAM and SAH bind to the same binding site on PRMT1, product inhibition with SAH is expected to demonstrate classic competitive inhibition when varying SAM. Second, with increasing concentrations of SAH and varying RKK peptide concentrations at 50 μM SAM, the data sets fit equally well to noncompetitive and mixed models (Table S3), which is also seen on each linear plot (Figure 5 C). In this case, the apparent V_{max} decreases and apparent K_M remains constant with increasing inhibitor concentration. An inhibition experiment with a high SAM concentration and varying RKK peptide was not conducted because it would not help distinguish between sequential ordered and random mechanisms. Overall, the results from SAH product inhibitor data sets were consistent with both a sequential ordered Bi–Bi mechanism and a rapid equilibrium random Bi–Bi mechanism with dead-end EAP/EBQ complexes. Further experiments with the RKK-aDMA product inhibitor were pursued to distinguish between these two mechanisms.

Table 5. Inhibition patterns for rapid equilibrium random mechanism with dead-end EAP/EBQ complexes and sequential ordered Bi–Bi mechanism under various SAM, peptide, SAH, and dimethylated peptide product concentrations.

	Varied SAM		Varied peptide	
Product inhibitor	Low peptide	High peptide	Low SAM	High SAM
Rapid equilibrium random mechanism (with dead-end EAP/EBQ)				
peptide product	mixed	no inhibition	competitive	competitive
SAH	competitive	competitive	mixed	no inhibition
Sequential ordered mechanism				
peptide product	mixed	uncompetitive	mixed	mixed
SAH	competitive	competitive	mixed	no inhibition

In Cleland notation, A refers to SAM, B is the unmethylated peptide, P is the methylated peptide, Q is SAH, and E is PRMT1.

Data sets corresponding to increasing RKK-aDMA inhibitor with varying SAM concentrations and 25 μM RKK peptide fit equally well to uncompetitive, noncompetitive, and mixed inhibition models (Table S3). As a consequence of assaying PRMT1 at this peptide concentration close to its K_M value, the resulting low activity of the enzyme contributed to error in these measurements. To aid in analysis, we looked to the linear plots, which demonstrate a noncompetitive/mixed inhibition pattern (Figure 6 A), consistent with both the random and sequential mechanisms. Together, these results best support that RKK-aDMA acts as a noncompetitive/mixed inhibitor towards PRMT1 under these conditions.

Next, with increasing concentrations of RKK-aDMA and varying SAM concentrations at 130 μM RKK peptide substrate ($\approx$10 K_M), the data sets fit best to the noncompetitive and mixed inhibition models. However, the data sets also fit appreciably well, with relatively low error, to the uncompetitive model (Table S3). Each plot is also consistent with this result in that it is difficult to confidently discern between a noncompetitive, mixed, or uncompetitive inhibition pattern when both apparent V_{max} and K_M values decreased with increasing inhibitor concentration (Figure 6 B). Taken together, this evidence best suggests that RKK-aDMA displays mixed/noncompetitive/uncompetitive inhibition under these conditions. Although it is difficult to assign a single inhibition model, it is important to remark that, under a sequential ordered mechanism, we would expect to see uncompetitive inhibition under these conditions, but under a rapid equilibrium random mechanism with dead-end EAP/EBQ complexes, we would expect to see no inhibition.[69]

Finally, with increasing concentrations of RKK-aDMA and various RKK concentrations at both 5.0 and 50 μM concentrations of SAM, these data sets reveal similarly low errors and coefficients of determination for noncompetitive and mixed inhibition models (Table S3), which is also consistently seen on the linear plots (Figure 6 C and D). These results, therefore, suggest that RKK-aDMA displayed mixed/noncompetitive inhibition

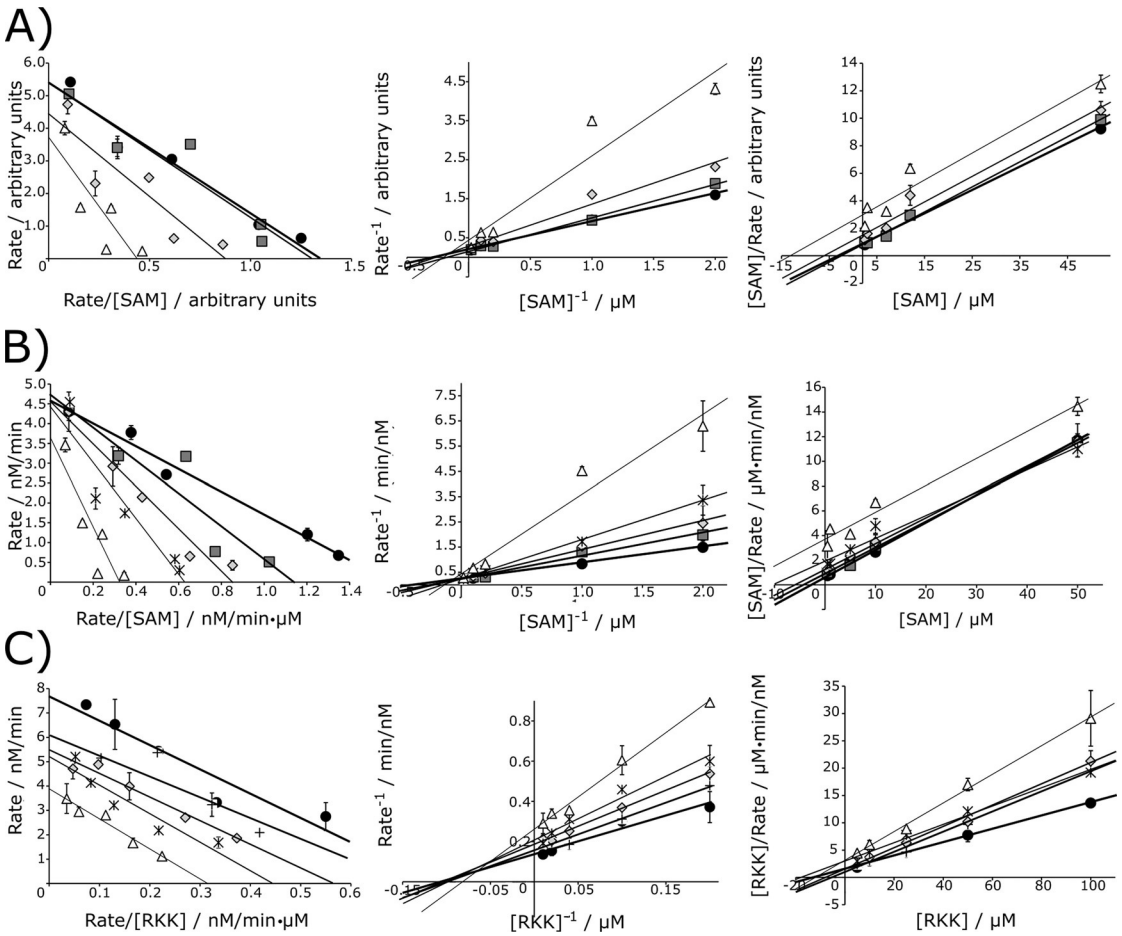

Figure 5. Product inhibitor results of PRMT1 with SAH inhibitor. Data are represented as Eadie–Hofstee (left; rate versus rate/variable substrate concentration), Lineweaver–Burk (middle; reciprocal rate versus reciprocal substrate concentration), and Hanes–Woolf (right; substrate/rate versus substrate concentration) plots. Linear regression analysis was applied to construct lines of best fit for the data. Methylation reactions containing 200 nM PRMT1 were carried out with different substrate and product inhibitor concentrations. Various concentrations of SAH used were 0 (●), 0.5 (■), 2.5 (+), 5.0 (◆), 10 (**x**), and 25 (△) μM. A) A constant concentration of RKK peptide (25 μM) was incubated with various SAH concentrations (as indicated) and various SAM concentrations (0.5, 1.0, 5.0, 10, or 50 μM). B) A constant concentration of RKK peptide (130 μM) was incubated with various SAH concentrations (as indicated) and various SAM concentrations (0.5, 1.0, 5.0, 10, or 50 μM). C) A constant concentration of SAM (50 μM) was incubated with various SAH concentrations (as indicated) and various RKK peptide concentrations (5.0, 10, 25, 50, or 100 μM). Some rates are reported in arbitrary units from disintegrations per minute (DPM). Error bars represent standard deviation ($n = 2$).

under these conditions. It is important to also discern that under a sequential ordered mechanism, we would expect to see mixed inhibition under these conditions, but under a rapid equilibrium random mechanism with dead-end EAP/EBQ complexes, we would expect to see competitive inhibition.[69] These data sets have much lower coefficients of determination when fit to the competitive model, accompanied by appreciably higher estimates of error. We also observed high K_i values in the range of 400 to 1000 μM for the RKK-aDMA inhibitor (Table S3), which suggests that RKK-aDMA is a weak PRMT1 inhibitor. Accordingly, large inhibitor concentrations were used.

The key difference between a rapid equilibrium random Bi–Bi mechanism with dead-end EAP/EBQ complexes and a sequential ordered Bi–Bi mechanism is whether or not substrate binding and product release occur in a random or ordered fashion. The latter mechanism has been assigned to PRMT2[11] and PRMT6,[42] whereas the former mechanism has been assigned to PRMT1,[36] CARM1,[38] PRMT5,[39] and PRMT6.[41] Our current nonlinear regression analyses and graphical representations provide the strongest evidence that PRMT1 operates by using a sequential ordered Bi–Bi mechanism instead of a rapid equilibrium random Bi–Bi mechanism with dead-end EAP/EBQ complexes. Specifically, if PRMT1 operated by using a rapid equilibrium random mechanism, we would have expected to see no inhibition when using the RKK-aDMA inhibitor with varied SAM concentration and a high RKK peptide concentration, but these conditions unquestionably showed inhibition. Furthermore, we would have expected to see competitive inhibition by RKK-aDMA when varying RKK peptide concentration, but both nonlinear and linear regression analyses revealed mixed/noncompetitive inhibition under these conditions. Therefore, results from our steady-state kinetic product inhibition experiments imply that it is more probable that PRMT1 uses a sequential ordered Bi–Bi mechanism rather than a random mechanism.

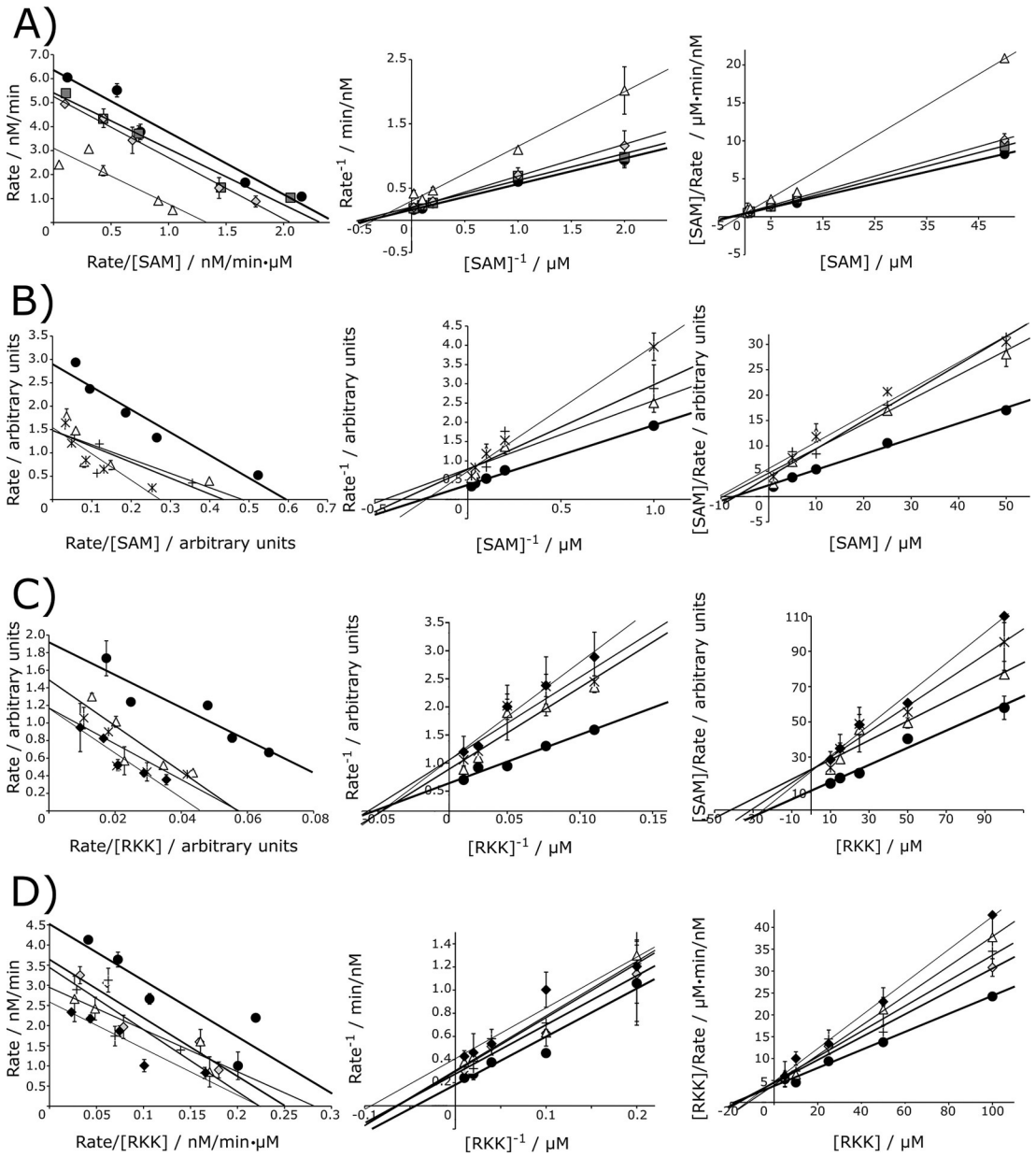

Figure 6. Product inhibitor results of PRMT1 with RKK-aDMA inhibitor. Data are represented as Eadie-Hofstee (left; rate versus rate/variable substrate concentration), Lineweaver–Burk (middle; reciprocal rate versus reciprocal substrate concentration), and Hanes-Woolf (right; substrate/rate versus substrate concentration) plots. Linear regression analysis was applied to construct lines of best fit for the data. Methylation reactions containing 200 nM PRMT1 were performed with different substrate and product inhibitor concentrations. Various concentrations of RKK-aDMA used were 0 (●), 100 (■), 300 (◆), 450 (+), 600 (△), 800 (**x**), and 1000 (◆) μM. A) A constant concentration of RKK peptide (25 μM) was incubated with various RKK-aDMA concentrations (as indicated) and various SAM concentrations (0.5, 1.0, 5.0, 10, or 50 μM). B) A constant concentration of RKK peptide (130 μM) was incubated with various RKK-aDMA concentrations (as indicated) and various SAM concentrations (1.0, 5.0, 10, 25, or 50 μM). C) A constant concentration of SAM (5.0 μM) was incubated with various RKK-aDMA concentrations (as indicated) and various RKK peptide concentrations (10, 15, 25, 50, or 100 μM). D) A constant concentration of SAM (50 μM) was incubated with various RKK-aDMA concentrations (as indicated) and various RKK peptide concentrations (5.0, 10, 25, 50, or 100 μM). Some rates are reported in arbitrary units from DPM. Error bars represent standard deviation ($n=2$).

Our product inhibition results contrast with findings from other studies.[36,38,39,41] The source of this discrepancy resides in the interpretation of product inhibition or dead-end inhibition curves involving peptide inhibitors (for example, RKK-aDMA). One issue that groups have encountered is high K_i values for inhibitor peptides, which require high enough concentrations to elicit inhibitory effects that can be accurately measured and properly interpreted. Another issue is reliance on Lineweaver–Burk double reciprocal plots, which tend to yield unequal weighting of data points over a range of substrate concentrations. Eadie–Hofstee and Hanes–Woolf plots, on the other hand, more evenly distribute data points so that patterns can be more readily discernible by visual inspection. We found in our own data that, in some instances, single plots were not able to clearly elucidate an inhibition pattern. For example, when using the RKK-aDMA inhibitor and various RKK concen-

trations at a low SAM concentration (Figure 6C), the Lineweaver–Burk plot appears unclear and could suggest an uncompetitive pattern. However, in this instance, both the Eadie–Hofstee and Hanes–Woolf plots strongly suggest a mixed inhibition pattern. This example demonstrates how the double reciprocal plot can be subject to user interpretation and further emphasizes the importance of assessing all plots as a complement to nonlinear regression and as an interpretive tool. Finally, the transformation of nonlinear kinetic models [Eqs. (3)–(6)] to a linear plot like the double reciprocal plot allows for visual inspection of the model rather than the acquired product inhibition data. In this instance, line patterns are not reflective of data points and are forced through a single *x*- or *y*-intercept, as seen in some PRMT studies.[39,41] Furthermore, it is surprising that regression metrics are not regularly reported in literature. This information would not only provide more robust support for authors' claims, but would also invite transparency and allow readers to draw their own conclusions from the presented data. The evaluation of product and dead-end inhibition studies does bear some pitfalls for misinterpretation of kinetic data, but they can be overcome when considering these issues.

Zheng and co-workers used transient kinetic measurements to establish a PRMT1 kinetic mechanism in which both SAM and histone H4 peptide were capable of independently binding to the enzyme, but the catalytically active ternary complex (PRMT1:SAM:H4) required that SAM bound first to PRMT1 before the peptide bound.[32] We were also able to conclude that cofactor and peptide could independently bind to PRMT1 when measuring dimerization by FRET (Figure 4). As we observed that some substrates led to enzyme inhibition at high concentrations (Figure 1), we questioned if this was due to the formation of dead-end EBQ, BEB, or BE complexes. The EBQ dead-end complex would be formed when the peptide substrate bound to the catalytically inactive PRMT1:SAH complex. The latter complexes would be theoretically formed when one or two peptide substrates bound to PRMT1 (BE and BEB, respectively) and prevented cofactor binding. To distinguish between these dead-end complexes, we conducted a series of experiments with various concentrations of H4-OH peptide (2, 5, 10, 25, 50, and 100 μM) and various concentrations of SAM (1, 2, 5, 10, and 50 μM). A double reciprocal plot of reciprocal rate versus reciprocal SAM concentration was used to reveal which dead-end complexes were formed.[70] We observe that, at low H4-OH concentrations (1–25 μM), the data sets intersect on the *x*-axis and share the same apparent K_M value, but at high H4-OH peptide concentrations (50–100 μM), the data sets intersect along the *y*-axis and share the same apparent V_{max} value (Figure 7A and Table S4). This pattern is characteristic of the formation of dead-end BE and BEB complexes. If we were observing inhibition by the formation of EBQ complexes, we would expect to see a decrease in K_M/V_{max} to a minimum as substrate concentrations increase. After this point, data sets at higher substrate concentrations would maintain the minimum K_M/V_{max}, but would show an increasing reciprocal rate.[70] Therefore, our evidence does not support the formation of an EBQ complex as an underlying mechanism for observed substrate inhibition.

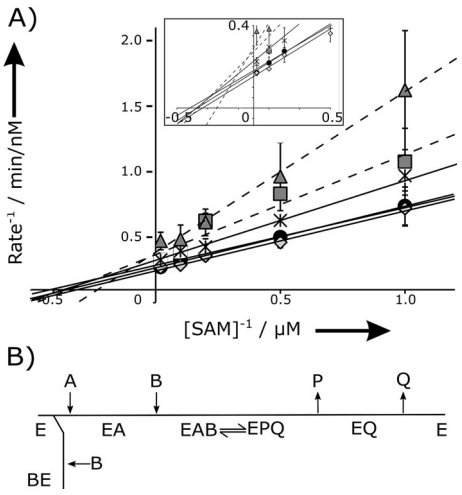

Figure 7. Hydroxy-substituted H4 peptide inhibits PRMT1 activity through formation of a dead-end BE complex. A) Data are represented in a Lineweaver–Burk (reciprocal rate versus reciprocal substrate concentration) plot. Linear regression analysis was applied to construct lines of best fit for the data. Methylation reactions containing 200 nM PRMT1 were carried out with varying SAM and H4-OH substrate concentrations. Various concentrations of H4-OH used were 2.0 (+), 5.0 (●), 10 (◆), 25 (x), 50 (■), and 100 μM (▲). Various concentrations of SAM used were 1, 2, 5, 10, and 50 μM. Inset: Zoomed-in view to observe intersecting lines along the *x*-axis (2, 5, 10, and 25 μM; ——) and *y*-axis (50 and 100 μM; -----). Error bars represent standard deviation ($n=2$). B) Cleland notation for a sequential ordered reaction mechanism with a dead-end BE complex in which A is SAM, B is the peptide substrate, P is the methylated peptide product, Q is SAH, and E is PRMT1.

In considering other mechanisms for substrate inhibition, it is important to note that the two substrate binding sites in PRMT1 are not mutually exclusive, as a dead-end BEB complex would suggest. For a BEB complex to form, A (SAM) and B (peptide) must be structurally similar in order for B to indiscriminately bind the enzyme at A and B binding sites. This mode of substrate inhibition seems unlikely, as no additional evidence exists to support such a mechanism. The alternative mechanism supported by kinetic data (Figure 7A) is formation of the dead-end BE complex, in which peptide binds the enzyme at the B binding site, such that binding of A is prevented from occurring. This mechanism for PRMT1 substrate inhibition seems logical, as the SAM binding site is occluded by an occupied peptide binding groove and inhabits a space contiguous to the arginine binding pocket, as observed in various PRMT crystal structures. These results, therefore, support the formation of a dead-end BE complex as an explanation for substrate inhibition observed within the oligomeric enzyme states that exist under low enzyme concentrations.

Despite the possibility of peptide binding first, the model presented by Zheng et al. and the evidence we present here both support the sequential ordered Bi–Bi mechanism for PRMT1. In their model, formation of a PRMT1:H4 complex was deemed catalytically inconsequential to methylation.[32] Here, we demonstrate that the formation of a BE complex prevents productive cofactor binding. This kinetic mechanism is further supported by published ITC data suggesting that peptide substrates do not readily bind PRMTs in the apo form,[30–32] as well

as structural data that provide visual evidence for cofactor binding as a prerequisite to peptide docking.[25–29]

Conclusion

Our study reveals that PRMT1 enzyme kinetics are largely dependent on substrate sequence, enzyme processivity is a multifactorial effect, and PRMT1 uses a sequential ordered Bi–Bi kinetic mechanism. These results have many implications for the field. Future research into PRMT processivity needs to consider the effect of enzyme and cofactor concentration on perceived enzyme dimerization and processivity. The processive nature of PRMT1 at high enzyme concentrations, however, might not be representative of conditions within a biological system. Furthermore, our data demonstrate the importance of using multiple linear plots as a complement to nonlinear analyses when interpreting kinetic data. The conflicting reports, therefore, might indicate previous misinterpretations that could be rectified through a more robust analysis of product inhibitor data sets. Our own results support published biophysical data that, although PRMTs can bind peptide substrate in the absence of cofactor, productive methylation is only accomplished if the peptide substrate binds in the presence of cofactor. In light of our findings and the structural and catalytic similarities between PRMT family members, we surmise that these enzymes share a common mechanism.

Experimental Section

Peptides: The various PRMT1 substrate peptides (Table 1 and Table S1) were prepared following standard Fmoc solid-phase peptide synthesis (SPPS) protocols. The requisite *N*η-hydroxy-L-arginine and *N*η-methyl-L-arginine building blocks were prepared as previously described.[58] Peptides were assembled on 2-chlorotrityl resin (0.25 mmol scale). With the exception of the modified L-arginine building blocks, peptide couplings were performed by using protected Fmoc amino acid (4.0 equiv), BOP reagent (4.0 equiv), and DIPEA (8.0 equiv) in DMF (total volume 10 mL) at ambient temperature for 1 h. Alternatively, incorporation of the modified L-arginine building residues was performed by using modified L-arginine building blocks (2.0 equiv), BOP reagent (2.0 equiv), and DIPEA (4.0 equiv) in DMF (total volume 10 mL) at ambient temperature overnight. Peptide couplings were verified by using the Kaiser and Bromophenol Blue tests. Upon completion of SPPS, peptides were cleaved from the resin and deprotected by using TFA/TIS/H_2O (95:2.5:2.5), followed by Et_2O precipitation to yield the crude peptides. Each peptide was purified to homogeneity by RP-HPLC, and its identity was confirmed by MS analysis.

The absorbance at 280 nm was used to estimate the concentrations of KRK, RKK, and R1 peptide solutions by using an extinction coefficient of 5500 M^{-1} cm^{-1} for KRK and RKK, and 13980 M^{-1} cm^{-1} for R1. The absorbance at 205 nm was used to estimate the concentrations of H4 and eIF4A1 peptides by using an extinction coefficient of 31 mg mL^{-1} cm^{-1}.[71] The monomethylated and asymmetrically dimethylated RKK peptides were purchased from Canada Peptide.

Expression and purification of PRMT1: A rat PRMT1 H161Y mutant was used as humanized PRMT1.[50] Construction of the pET28a(+)-His_6-PRMT1 and pET28a(+)-mCerulean/mCitrine-His_6-PRMT1 plasmids was previously described, and PRMT1 (UniProt Accession ID: Q99873) proteins were expressed and purified according to established protocols.[50] Briefly, the plasmids were transformed into BL21(DE3) plysS (Stratagene) cells, and protein expression was induced at an OD_{600} of 0.8 with isopropyl β-D-1-thiogalactopyranoside (IPTG; 1.0 mM) at 30 °C with shaking at 250 rpm for 16 h. Cells were harvested by centrifugation at 10000 *g* for 15 min at 4 °C, and cell pellets were frozen at −80 °C. Thawed pellets were resuspended in lysis buffer (2 mL lysis buffer per gram of cell pellet): HEPES·KOH (50 mM, pH 7.6), NH_4Cl (1.0 M), $MgCl_2$ (10 mM), Triton X-100 (0.1%, *v/v*), lysozyme (0.1%, *w/v*), DNAse 1 (25 U mL^{-1}), β-mercaptoethanol (β-Me; 7.0 mM), phenylmethanesulphonyl fluoride (PMSF; 1.0 mM), and EDTA-free protease inhibitor cocktail (1.0 mM; Roche: 04693132001). Cells were further lysed at 4 °C by using a Branson Sonifier 450 with eight 30 s pulses at 50% duty cycle with 30 s pauses. The lysate was clarified through centrifugation at 35000 *g* for 1 h at 4 °C and filtered through 0.45 μm low protein binding Durapore membrane (Millipore). The lysate was applied to a pre-equilibrated HisTrap FF column (GE Healthcare) with wash buffer [HEPES (50 mM, pH 7.6), NH_4Cl (1.0 M), $MgCl_2$ (10 mM), β-Me (7 mM), imidazole (10 mM), PMSF (1 mM)]. The bound fraction was eluted by using the same buffer with imidazole (400 mM) added. Eluted fractions containing PRMT1 were pooled and applied to a pre-equilibrated HiLoad 26/600 Superdex 200 pg size-exclusion column (GE Healthcare) column. His_6-PRMT1 was applied by using a Tris running buffer [Tris·HCl (50 mM, pH 7.5), NaCl (100 mM)]. Eluted fractions were pooled and concentrated by using Amicon Ultra 15 mL filters with 30 K molecular weight cut-off (MWCO; Millipore). Fractions appeared to be greater than 90% pure (Figure S1). His_6-PRMT1 was further exchanged into storage buffer [HEPES·KOH (100 mM, pH 8), NaCl (200 mM), DTT (1 mM), glycerol (10%), and EDTA (2 mM)].

The concentration of His_6-PRMT1 was estimated according to the Edelhoch method, in which absorbance at 280 nm of the denatured protein was measured in guanidine·HCl (6.6 M) in potassium phosphate buffer (40 mM, pH 6.5).[72] Concentrations of mCit- and mCer-PRMT1 were quantified by measuring the absorbance of the protein at 516 and 434 nm, respectively, and with extinction coefficients of 77000 and 43000 M^{-1} cm^{-1}, respectively.[73]

PRMT1 Michaelis–Menten enzyme kinetics: *P81 filter binding assay*: Reactions containing PRMT1 (200 nM), *S*-adenosyl-L-[methyl-^{14}C]-methionine ([^{14}C]SAM; 58 mCi $mmol^{-1}$ in H_2SO_4/ethanol (9:1, 10 mM); PerkinElmer NEC363050UC; 50 μM), and increasing concentrations of unmethylated, monomethylated, or hydroxylated substrate peptide (0.5–100 μM) were incubated for 1 h at 37 °C in methylation buffer [HEPES (50 mM, pH 8.0), NaCl (10 mM), DTT (1.0 mM); total volume: 27 μL]. The linear range was determined by incubating PRMT1 (200 nM) and [^{14}C]SAM (50 μM) with each unmodified peptide (100 μM) for 20–180 min (Figure S2). A P81 filter binding assay was used to measure PRMT1 activity in the presence of substrate, in which the positively charged peptides were immobilized onto Whatman P81 phosphocellulose filter paper (Fisher Scientific 3698-915).[74] Each reaction was spotted (12 μL) onto the filter paper in duplicate and dried at ambient temperature (25 °C). Dry filter papers were washed by vortexing and gentle shaking five times in sodium carbonate-bicarbonate buffer (pH 9.0, 5 mL) for 5 min each time in culture tubes (Sarstedt 62.515.006). Filter papers were dried overnight at 37 °C. Dry filter papers were transferred to 6 mL scintillation vials (PerkinElmer PA6000292) with Scintiverse E scintillation cocktail (2.5 mL; Fisher Scientific SX16-4). Disintegrations per minute (DPM) of the samples were quantified for 1 min by using a Tri-Carb 3110TR (PerkinElmer) liquid scintillation

counter. Linear ranges were determined by plotting methyl transfer versus time. The observed reaction rates were fitted to the Michaelis–Menten equation (1) or Michaelis–Menten substrate inhibition equation (2) by using SigmaPlot 12 (Systat), from which the apparent K_M, k_{cat}, V_{max}, and standard error values were estimated.

$$v = (V_{max}[S])/(K_M + [S]) \quad (1)$$

$$v = (V_{max}[S])/(K_M + [S](1 + [S]/K_i)) \quad (2)$$

Radioactive tricine gel assay: In order to estimate apparent PRMT1 enzyme kinetics with the R1 peptide, a radioactive gel assay was used. Reactions containing PRMT1 (200 nM), [^{14}C]SAM (50 μM), and R1 peptide (0–100 μM) in methylation buffer (total volume: 100 μL) were incubated for 1 h at 37 °C. Reactions were concentrated by using a Savant ISS110 SpeedVac Concentrator (Thermo Scientific) on high temperature and speed for 1 h. Reactions were reconstituted in tricine sample buffer (32 μL; Tris·HCl (50 mM, pH 6.8), glycerol (13%), SDS (0.2%), Coomassie Brilliant Blue G-250 (0.02%), and β-mercaptoethanol (0.4%)]. After loading each reaction (15 μL) in duplicate on a tricine gel (16.5%), sample proteins and peptides were electrophoretically separated. After separation, peptides were fixed in gels by using glutaraldehyde (5%) in boric acid (0.5 M, pH 6.2). The gels were stained with Coomassie Brilliant Blue (0.025%). Each lane was excised and dissolved in hydrogen peroxide (30%, total volume: 4 mL) at 70 °C for 4 h in 20 mL scintillation vials (PerkinElmer 6000477).[75] Afterwards, Scintiverse E scintillation cocktail (10 mL) was added, and the mixture was stirred until a gel formed. The DPM of each sample was measured, and apparent enzyme kinetic parameters were estimated as described above.

Peptide methylation analyses by mass spectrometry: Methylation reactions containing PRMT1, SAM (in 0.5 mM HCl), and unmodified peptide in methylation buffer were incubated for 1 h at 37 °C. To stop the reaction and remove confounding automethylation, PRMT1 was separated from reactions by filtration through a 30 K MWCO filtration device (VWR 82031-352) that was prewashed with deionized water (1 mL). Reactions were then transferred to 6×50 mm Pyrex glass tubes (Corning 9820-6) and dried in a Savant ISS110 SpeedVac Concentrator on high temperature and speed for 1.5 h. Dried reaction tubes were transferred to a reaction vial assembly (Eldex 1163), with HCl (6 N, 200 μL) in the bottom of the reaction vial. Samples were acid hydrolyzed in vacuo for 20–24 h at 110 °C by using a Waters Pico Tag work station. Each reaction was resuspended in mobile phase A [100 μL; formic acid (0.1%) and trifluoroacetic acid (TFA; 0.05%) in water], and all insoluble debris was removed by centrifugation to enable UHPLC-MS/MS analysis of MMA and aDMA production.

The UHPLC-MS/MS procedure closely followed a previously described method.[11] A Water Acquity UHPLC bridged ethylene hybrid C_{18} column (2.1 mm×100 mm) was used at a flow rate of 0.15 mL min^{-1} at 45 °C. Mobile phase A (described above) and mobile phase B [formic acid (0.1%), TFA (0.05%), and methanol (30%) in water] were used in a linear gradient of 0–100% phase B over 2.90 min. A Linear Ion Trap Quadrupole QTRAP 5500 mass spectrometer (Sciex 1024945-AM) was operated in positive-ion mode with electrospray ionization in multiple reaction monitoring mode to detect parent and product ions of MMA and aDMA. For MMA, a cone voltage of 30 V and 17 eV collision energy was used to detect the parent ion (189 *m/z*) and product ion (74 *m/z*). For aDMA, a 30 V cone voltage and 20 eV collision energy were used to detect the parent ion (203 *m/z*) and product ion (46 *m/z*). A sample injection volume of 5.0 μL was used. MMA and aDMA standards were initially reconstituted in deionized water and were diluted in mobile phase A to prepare linear standard curves (0.02–5.0 μM). Concentrations of MMA and aDMA present in each reaction were interpolated from the standard curves, and the aDMA/MMA ratios were calculated.

To observe methylation ratios of unmodified peptides under conditions used in the Michaelis–Menten enzyme kinetic assays, PRMT1 (200 nM), SAM (50 μM), and each peptide (100 μM) were incubated (total volume: 60 μL) at 37 °C for 1 h. Reactions were subsequently subjected to PRMT1 removal, acid hydrolysis, and UHPLC-MS/MS analysis. To observe methylation ratios of unmodified peptides with variable substrate concentrations, all reactions contained PRMT1 (5.0 μM) and one of the following conditions: limiting SAM (1.0 μM) and excess substrate, corresponding to a concentration at least ten times higher than the K_M value of each peptide (25 μM for H4, 300 μM for eIF4A1, 35 μM for KRK, and 130 μM for RKK); intermediate SAM (10 μM) and excess substrate; or limiting peptide substrate (10 μM), and excess SAM (100 μM) in triplicate (total volume: 60 μL). To observe methylation ratios of unmodified peptides with increasing enzyme concentrations, reactions contained constant saturating concentrations of SAM (100 μM), substrate concentrations at least ten times higher than the K_M value as before, and varying PRMT1 concentrations (0.2, 1.0, or 5.0 μM) in at least duplicate (total volume: 60 μL).

FRET assay: Reactions containing mCerulean-PRMT1 (100 nM; mCer-PRMT1) and mCitrine-PRMT1 (100 nM; mCit-PRMT1) fluorescent proteins in methylation buffer were incubated with varying concentrations of KRK peptide, SAM, or SAH (0, 2.5, 5.0, 10, 20, 40, 50 μM) at 37 °C for 1 h (80 μL initial volume; the buffer-only control showed that small changes to the volume from the addition of stock solutions had a negligible impact on changes to FRET signal). Reactions were also prepared containing varying KRK peptide concentrations in the presence of SAM (50 μM) and varying SAM concentrations in the presence of KRK peptide (50 μM). PRMT1 dimerization was assessed by exciting reactions in individual wells in a 384-well black polystyrene non-binding surface microplate (Corning #3575) at 434 nm and measuring the fluorescence at 475 and 529 nm by using a Synergy MX microplate reader (BioTek) with excitation and emission slit widths of 9 nm and sensitivity adjusted with an 8 mm height correction from the upper plane of the sample wells. The ratios of fluorescence at 529 nm and 475 nm were calculated to measure FRET for each equilibrated reaction mixture.

PRMT1 product and substrate inhibition: A radioactive P81 filter binding assay (described above) was used to determine the kinetic mechanism of PRMT1 by using SAM or RKK substrate with SAH or RKK-aDMA inhibitor and PRMT1 (200 nM) in methylation buffer. Assays that contained constant RKK peptide (25 or 130 μM) were performed with various SAM (0.5, 1.0, 5.0, 10, 25, 50 μM) and various SAH (0, 0.5, 2.0, 5.0, 10, 25 μM) or various RKK-aDMA (300, 450, 600, 800, 1000 μM) concentrations. Assays that contained constant SAM (5.0 or 50 μM) were performed with various RKK peptide (5.0, 10, 15, 25, 50, 100 μM) and variable SAH (0, 0.5, 2.0, 5.0, 10, 25 μM) or various RKK-aDMA (300, 450, 600, 800, 1000 μM) concentrations. Data were interpreted through both quantitative nonlinear and qualitative linear analyses. For quantitative analysis, each data set was fit to equations corresponding to competitive [Eq. (3)], uncompetitive [Eq. (4)], noncompetitive [Eq. (5)], and mixed [Eq. (6)] inhibition by using SigmaPlot 12 (Systat Software, Inc.),

$$v = \frac{V_{max}[S]}{K_M(1 + [I]/K_i) + [S]} \quad (3)$$

$$v = \frac{V_{max}[S]}{K_M + [S](1 + [I]/K_i)} \quad (4)$$

$$v = \frac{V_{max}[S]}{K_M(1 + [I]/K_i) + [S](1 + [I]/K_i)} \quad (5)$$

$$v = \frac{V_{max}[S]}{K_M(1 + [I]/K_{ia}) + [S](1 + [I]/K_{ib})} \quad (6)$$

in which V_{max} and K_M were held constant. Best fitting of the data was determined by comparing standard errors of the fits. For qualitative analysis, Eadie–Hofstee [Eq. (7)], Lineweaver–Burk [Eq. (8)], and Hanes–Woolf [Eq. (9)] plots were generated directly from product inhibition data sets by using linear regression (i.e., transformations of nonlinear models were not employed). These linear plots were used to visualize data and supplement nonlinear analyses.

$$v = \frac{V_{max}}{1 + [I]/K_{ib}} - \frac{(1 + [I]/K_{ia})K_M}{1 + [I]/K_{ib}} \frac{v}{[S]} \quad (7)$$

$$\frac{1}{v} = \frac{(1 + [I]/K_{ia})K_M}{V_{max}} \frac{1}{[S]} + \frac{1 + [I]/K_{ib}}{V_{max}} \quad (8)$$

$$\frac{[S]}{v} = \frac{1 + [I]/K_{ib}}{V_{max}}[S] + \frac{(1 + [I]/K_{ia})K_M}{V_{max}} \quad (9)$$

A radioactive P81 filter binding assay was similarly used to observe substrate inhibition of PRMT1 (200 nM) by using various concentrations of H4-OH substrate peptide (2, 5, 10, 25, 50, and 100 μM) with various concentrations of SAM (1, 2, 5, 10, and 50 μM). A Lineweaver–Burk [Eq. (8)] plot was directly generated from the data and used to observe apparent enzyme kinetic parameters under such conditions.

Acknowledgements

We thank András Szeitz for providing mentorship and expertise in mass spectrometry. This work was supported by the Natural Sciences and Engineering Research Council of Canada (NSERC) RGPIN-2015–04450 Discovery Grant (A.F.), NSERC CGS-M (J.I.B.), the Shaughnessy Hospital Volunteer Society Fellowship in Health Care (J.I.B.), and the Walter C. Koerner Fellowship (J.I.B.). Additional support provided by Utrecht University and the Netherlands Organization for Scientific Research is acknowledged (T.K., J.v.S., and N.I.M.).

Conflict of Interest

The authors declare no conflict of interest.

Keywords: enzyme catalysis · kinetics · peptides · protein modifications · transferases

[1] R. S. Blanc, S. Richard, *Mol. Cell* **2017**, *65*, 8 – 24.
[2] M. Matsuoka, *Seikagaku* **1972**, *44*, 364 – 370.
[3] W. K. Paik, S. Kim, *Natural Occurrence of Various Methylated Amino Acid Derivatives*, Wiley, New York, **1975**.
[4] B. Chang, Y. Chen, Y. Zhao, R. K. Bruick, *Science* **2007**, *318*, 444 – 447.
[5] A. Böttger, M. S. Islam, R. Chowdhury, C. J. Schofield, A. Wolf, *Biochem. J.* **2015**, *468*, 191 – 202.
[6] A. Frankel, N. Yadav, J. Lee, T. L. Branscombe, S. Clarke, M. T. Bedford, *J. Biol. Chem.* **2002**, *277*, 3537 – 3543.
[7] C. I. Zurita-lopez, T. Sandberg, R. Kelly, S. G. Clarke, *J. Biol. Chem.* **2012**, *287*, 7859 – 7870.
[8] W. J. Lin, J. D. Gary, M. C. Yang, S. Clarke, H. R. Herschman, *J. Biol. Chem.* **1996**, *271*, 15034 – 15044.
[9] D. Chen, H. Ma, H. Hong, S. S. Koh, S. M. Huang, B. T. Schurter, D. W. Aswad, M. R. Stallcup, *Science* **1999**, *284*, 2174 – 2177.
[10] J. Tang, J. D. Gary, S. Clarke, H. R. Herschman, *J. Biol. Chem.* **1998**, *273*, 16935 – 16945.
[11] T. M. Lakowski, A. Frankel, *Biochem. J.* **2009**, *421*, 253 – 261.
[12] T. L. Branscombe, A. Frankel, J. H. Lee, J. R. Cook, Z. H. Yang, S. Pestka, S. Clarke, *J. Biol. Chem.* **2001**, *276*, 32971 – 32976.
[13] J. Lee, J. Sayegh, J. Daniel, S. Clarke, M. T. Bedford, *J. Biol. Chem.* **2005**, *280*, 32890 – 32896.
[14] J. R. Cook, J. H. Lee, Z. H. Yang, C. D. Krause, N. Herth, R. Hoffmann, S. Pestka, *Biochem. Biophys. Res. Commun.* **2006**, *342*, 472 – 481.
[15] S. Gui, W. L. Wooderchak, M. P. Daly, P. J. Porter, S. J. Johnson, J. M. Hevel, *J. Biol. Chem.* **2011**, *286*, 29118 – 29126.
[16] S. Gui, S. Gathiaka, J. Li, J. Qu, O. Acevedo, J. M. Hevel, *J. Biol. Chem.* **2014**, *289*, 9320 – 9327.
[17] S. Gathiaka, B. Boykin, T. Cáceres, J. M. Hevel, O. Acevedo, *Bioorg. Med. Chem.* **2016**, *24*, 4949 – 4960.
[18] E. W. Debler, K. Jain, R. A. Warmack, Y. Feng, S. G. Clarke, G. Blobel, P. Stavropoulos, *Proc. Natl. Acad. Sci. USA* **2016**, *113*, 2068 – 2073.
[19] K. Jain, R. A. Warmack, E. W. Debler, A. Hadjikyriacou, P. Stavropoulos, S. G. Clarke, *J. Biol. Chem.* **2016**, *291*, 18299 – 18308.
[20] X. Zhang, X. Cheng, *Structure* **2003**, *11*, 509 – 520.
[21] M. L. Pak, T. M. Lakowski, D. Thomas, M. I. Vhuiyan, K. Hüsecken, A. Frankel, *Biochemistry* **2011**, *50*, 8226 – 8240.
[22] Y. H. Lee, S. S. Koh, X. Zhang, X. Cheng, M. R. Stallcup, *Mol. Cell. Biol.* **2002**, *22*, 3621 – 3632.
[23] H. Wu, W. Zheng, M. S. Eram, M. Vhuiyan, A. Dong, H. Zeng, H. He, P. Brown, A. Frankel, M. Vedadi, M. Luo, J. Min, *Biochem. J.* **2016**, *473*, 3049 – 3063.
[24] T. C. Petrossian, S. G. Clarke, *Mol. Cell. Proteomics* **2009**, *8*, 1516 – 1526.
[25] W. W. Yue, M. Hassler, S. M. Roe, V. Thompson-Vale, L. H. Pearl, *EMBO J.* **2007**, *26*, 4402 – 4412.
[26] N. Troffer-Charlier, V. Cura, P. Hassenboehler, D. Moras, J. Cavarelli, *EMBO J.* **2007**, *26*, 4391 – 4401.
[27] J. S. Sack, S. Thieffine, T. Bandiera, M. Fasolini, G. J. Duke, L. Jayaraman, K. F. Kish, H. E. Klei, A V. Purandare, P. Rosettani, S. Troiani, D. Xie, J. A. Bertrand, *Biochem. J.* **2011**, *436*, 331 – 339.
[28] L. Bonnefond, J. Stojko, J. Mailliot, N. Troffer-Charlier, V. Cura, J. M. M. Wurtz, S. Cianférani, J. Cavarelli, *J. Struct. Biol.* **2015**, *191*, 175 – 183.
[29] P. A. Boriack-Sjodin, L. Jin, S. L. Jacques, A. Drew, C. Sneeringer, M. P. Scott, M. P. Moyer, S. Ribich, O. Moradei, R. A. Copeland, *ACS Chem. Biol.* **2016**, *11*, 763 – 771.
[30] C. Wang, Y. Zhu, J. J. Chen, X. Li, J. Peng, J. J. Chen, Y. Zou, Z. Zhang, H. Jin, P. Yang, J. Wu, L. Niu, Q. Gong, M. Teng, Y. Shi, *PLoS One* **2014**, *9*, e87267.
[31] C. Wang, Y. Zhu, T. B. Caceres, L. Liu, J. Peng, J. Wang, J. Chen, X. Chen, Z. Zhang, X. Zuo, Q. Gong, M. Teng, J. M. Hevel, J. Wu, Y. Shi, *Structure* **2014**, *22*, 756 – 768.
[32] H. Hu, C. Luo, Y. G. Zheng, *J. Biol. Chem.* **2016**, *291*, 26722 – 26738.
[33] M. S. Eram, Y. Shen, M. Szewczyk, H. Wu, G. Senisterra, F. Li, K. V. Butler, H. Ü. Kaniskan, B. A. Speed, C. dela Seña, A. Dong, H. Zeng, M. Schapira, P. J. Brown, C. H. Arrowsmith, D. Barsyte-Lovejoy, J. Liu, M. Vedadi, J. Jin, *ACS Chem. Biol.* **2016**, *11*, 772 – 781.
[34] Y. Shen, M. M. Szewczyk, M. S. Eram, D. Smil, H. Ü. Kaniskan, R. Ferreira De Freitas, G. Senisterra, F. Li, M. Schapira, P. J. Brown, C. H. Arrowsmith, D. Barsyte-Lovejoy, J. Liu, M. Vedadi, J. Jin, *J. Med. Chem.* **2016**, *59*, 9124 – 9139.
[35] Y. Feng, N. Xie, M. Jin, M. R. Stahley, J. T. Stivers, Y. G. Zheng, *Biochemistry* **2011**, *50*, 7033 – 7044.
[36] O. Obianyo, T. C. Osborne, P. R. Thompson, *Biochemistry* **2008**, *47*, 10420 – 10427.
[37] H. L. Rust, C. I. Zurita-Lopez, S. Clarke, P. R. Thompson, *Biochemistry* **2011**, *50*, 3332 – 3345.
[38] S. L. Jacques, K. P. Aquino, J. Gureasko, P. A. Boriack-Sjodin, M. Porter Scott, R. A. Copeland, T. V. Riera, *Biochemistry* **2016**, *55*, 1635 – 1644.

[39] M. Wang, R. M. Xu, P. R. Thompson, *Biochemistry* **2013**, *52*, 5430 – 5440.
[40] L. Sun, M. Wang, Z. Lv, N. Yang, Y. Liu, S. Bao, W. Gong, R. M. Xu, *Proc. Natl. Acad. Sci. USA* **2011**, *108*, 20538 – 20543.
[41] O. Obianyo, P. R. Thompson, *J. Biol. Chem.* **2012**, *287*, 6062 – 6071.
[42] T. M. Lakowski, A. Frankel, *J. Biol. Chem.* **2008**, *283*, 10015 – 10025.
[43] X. Zhang, L. Zhou, X. Cheng, *EMBO J.* **2000**, *19*, 3509 – 3519.
[44] M. Hasegawa, S. Toma-Fukai, J. D. Kim, A. Fukamizu, T. Shimizu, *FEBS Lett.* **2014**, *588*, 1942 – 1948.
[45] W. C. Lee, W. L. Lin, T. Matsui, E. S. W. Chen, T. Y. W. Wei, W. H. Lin, H. Hu, Y. G. Zheng, M. D. Tsai, M. C. Ho, *Biochemistry* **2015**, *54*, 7514 – 7523.
[46] V. Cura, N. Marechal, N. Troffer-Charlier, J. M. Strub, M. J. van Haren, N. I. Martin, S. Cianferani, L. Bonnefond, J. Cavarelli, *FEBS J.* **2016**, *283*, 77 – 96.
[47] V. Cura, N. Troffer-Charlier, J. M. Wurtz, L. Bonnefond, J. Cavarelli, *Acta Crystallogr. Sect. D* **2014**, *70*, 2401 – 2412.
[48] V. H. Weiss, A. E. McBride, M. A. Soriano, D. J. Filman, P. A. Silver, J. M. Hogle, *Nat. Struct. Biol.* **2000**, *7*, 1165 – 1171.
[49] K. Higashimoto, P. Kuhn, D. Desai, X. Cheng, W. Xu, *Proc. Natl. Acad. Sci. USA* **2007**, *104*, 12318 – 12323.
[50] D. Thomas, T. M. Lakowski, M. L. Pak, J. J. Kim, A. Frankel, *Protein Sci.* **2010**, *19*, 2141 – 2151.
[51] T. Osborne, O. Obianyo, X. Zhang, X. Cheng, P. R. Thompson, *Biochemistry* **2007**, *46*, 13370 – 13381.
[52] K. M. Dorgan, W. L. Wooderchak, D. P. Wynn, E. L. Karschner, J. F. Alfaro, Y. Cui, Z. S. Zhou, J. M. Hevel, *Anal. Biochem.* **2006**, *350*, 249 – 255.
[53] S. Gui, W. L. Wooderchak-Donahue, T. Zang, D. Chen, M. P. Daly, Z. S. Zhou, J. M. Hevel, *Biochemistry* **2013**, *52*, 199 – 209.
[54] K. Kölbel, C. Ihling, K. Bellmann-Sickert, I. Neundorf, A. G. Beck-Sickinger, A. Sinz, U. Kühn, E. Wahle, *J. Biol. Chem.* **2009**, *284*, 8274 – 8282.
[55] M. Wang, J. Fuhrmann, P. R. Thompson, *Biochemistry* **2014**, *53*, 7884 – 7892.
[56] S. Antonysamy, Z. Bonday, R. M. Campbell, B. Doyle, Z. Druzina, T. Gheyi, B. Han, L. N. Jungheim, Y. Qian, C. Rauch, M. Russell, J. M. Sauder, S. R. Wasserman, K. Weichert, F. S. Willard, A. Zhang, S. Emtage, *Proc. Natl. Acad. Sci. USA* **2012**, *109*, 17960 – 17965.
[57] E. S. Burgos, C. Wilczek, T. Onikubo, J. B. Bonanno, J. Jansong, U. Reime, D. Shechter, *J. Biol. Chem.* **2015**, *290*, 9674 – 9689.
[58] D. Thomas, T. Koopmans, T. M. Lakowski, H. Kreinin, M. I. Vhuiyan, S. A. Sedlock, J. M. Bui, N. I. Martin, A. Frankel, *ChemBioChem* **2014**, *15*, 1607 – 1613.
[59] H. Wang, Z. Q. Huang, L. Xia, Q. Feng, H. Erdjument-Bromage, B. D. Strahl, S. D. Briggs, C. D. Allis, J. Wong, P. Tempst, Y. Zhang, *Science* **2001**, *293*, 853 – 857.
[60] S. Huang, M. Litt, G. Felsenfeld, *Genes Dev.* **2005**, *19*, 1885 – 1893.
[61] W. L. Wooderchak, T. Zang, Z. S. Zhou, M. Acuña, S. M. Tahara, J. M. Hevel, *Biochemistry* **2008**, *47*, 9456 – 9466.
[62] C. H. Lin, H. M. Huang, M. Hsieh, K. M. Pollard, C. Li, *J. Protein Chem.* **2002**, *21*, 447 – 453.
[63] Q. Liu, G. Dreyfuss, *Mol. Cell. Biol.* **1995**, *15*, 2800 – 2808.
[64] P. 't Hart, D. Thomas, R. van Ommeren, T. M. Lakowski, A. Frankel, N. I. Martin, *MedChemComm* **2012**, *3*, 1235 – 1244.
[65] M. B. C. Dillon, H. L. Rust, P. R. Thompson, K. A. Mowen, *J. Biol. Chem.* **2013**, *288*, 27872 – 27880.
[66] S. F. M. Van Dongen, J. A. A. W. Elemans, A. E. Rowan, R. J. M. Nolte, *Angew. Chem. Int. Ed.* **2014**, *53*, 11420 – 11428; *Angew. Chem.* **2014**, *126*, 11604 – 11612.
[67] R. Zhou, Y. Xie, H. Hu, G. Hu, V. S. Patel, J. Zhang, K. Yu, Y. Huang, H. Jiang, Z. Liang, Y. G. Zheng, C. Luo, *J. Chem. Inf. Model.* **2015**, *55*, 2623 – 2632.
[68] J. E. Dowd, D. S. Riggs, *J. Biol. Chem.* **1965**, *240*, 863 – 869.
[69] W. W. Cleland, *Adv. Enzymol. Relat. Areas Mol. Biol.* **1967**, 1 – 32.
[70] I. H. Segel, *Enzyme Kinetics: Behaviour and Analysis of Rapid Equilibrium and Stead-State Enzyme Systems*, Wiley, New York **1993**.
[71] R. K. Scopes, *Anal. Biochem.* **1974**, *59*, 277 – 282.
[72] H. Edelhoch, *Biochemistry* **1967**, *6*, 1948 – 1954.
[73] M. L. Markwardt, G. J. Kremers, C. A. Kraft, K. Ray, P. J. C. Cranfill, K. A. Wilson, R. N. Day, R. M. Wachter, M. W. Davidson, M. A. Rizzo, *PLoS One* **2011**, *6*, e17896.
[74] G. Blum, G. Ibáñez, X. Rao, D. Shum, C. Radu, H. Djaballah, J. C. Rice, M. Luo, *ACS Chem. Biol.* **2014**, *9*, 2471 – 2478.
[75] R. Young, H. Fulhorst, *Anal. Biochem.* **1965**, *11*, 389 – 391.

Manuscript received: September 28, 2017
Accepted manuscript online: November 7, 2017
Version of record online: November 29, 2017